

Computational study of inverse ferrite spinels

A EL Maazouzi, R Masrour, A Jabar, M Hamedoun

Citation: Chin. Phys. B . 2019, 28(5): 057504. **doi:** 10.1088/1674-1056/28/5/057504
Journal homepage: http://cpb.iphy.ac.cn; http://iopscience.iop.org/cpb

What follows is a list of articles you may be interested in

Phase diagrams and magnetic properties of the mixed spin-1 and spin-3/2 Ising ferromagnetic thin film:Monte Carlo treatment

B Boughazi, M Boughrara, M Kerouad
Chin. Phys. B . 2019, 28(2): 027501. **doi:** 10.1088/1674-1056/28/2/027501

Effect of particle size distribution on magnetic behavior of nanoparticles with uniaxial anisotropy

S Rizwan Ali, Farah Naz, Humaira Akber, M Naeem, S Imran Ali, S Abdul Basit, M Sarim, Sadaf Qaseem
Chin. Phys. B . 2018, 27(9): 097503. **doi:** 10.1088/1674-1056/27/9/097503

Typicality at quantum-critical points

Lu Liu(刘录), Anders W Sandvik, Wenan Guo(郭文安)
Chin. Phys. B . 2018, 27(8): 087501. **doi:** 10.1088/1674-1056/27/8/087501

Effect of exchange interaction in ferromagnetic superlattices: A Monte Carlo study

R Masrour, A Jabar
Chin. Phys. B . 2016, 25(10): 107502. **doi:** 10.1088/1674-1056/25/10/107502

Magnetocaloric and magnetic properties of La_2NiMnO_6 double perovskite

Masrour R, Jabar A
Chin. Phys. B . 2016, 25(8): 087502. **doi:** 10.1088/1674-1056/25/8/087502

Computational study of inverse ferrite spinels

A EL Maazouzi[1], R Masrour[1,†], A Jabar[1], and M Hamedoun[2]

[1] *Laboratory of Materials, Processes, Environment and Quality, Cadi Ayyad University, National School of Applied Sciences, Sidi Bouzid, Safi* 63 46000, *Morocco*

[2] *Institute of Nanomaterials and Nanotechnologies, MAScIR, Rabat, Morocco*

(Received 6 February 2019; revised manuscript received 5 March 2019; published online 4 April 2019)

The magnetic properties of inverse ferrite $\left(Fe^{3+}\right)\left[Fe^{3+}Co^{2+}\right]O_4^{2-}$, $\left(Fe^{3+}\right)\left[Fe^{3+}Cu^{2+}\right]O_4^{2-}$, $\left(Fe^{3+}\right)\left[Fe^{3+}Fe^{2+}\right]O_4^{2-}$, and $\left(Fe^{3+}\right)\left[Fe^{3+}Ni^{2+}\right]O_4^{2-}$ spinels have been studied using Monte Carlo simulation. We have also calculated the critical and Curie Weiss temperatures from the thermal magnetizations and inverse of magnetic susceptibilities for each system. Magnetic hysteresis cycles have been found for the four systems. Finally, we found the critical exponents associated with magnetization, magnetic susceptibility, and external magnetic field. Our results of critical and Curie Weiss temperatures are similar to those obtained by experiment results. The critical exponents are similar to those of known 3D-Ising model.

Keywords: inverse ferrites spinels, Monte Carlo simulation, critical and Curie Weiss temperatures, magnetic hysteresis cycles, critical exponents

PACS: 75.50.Gg, 75.40.Mg, 75.70.–i **DOI:** 10.1088/1674-1056/28/5/057504

1. Introduction

Cubic ferrite has the formula $M^{2+}Fe^{3+}O_4^{2-}$, where M is a divalent atom (e.g., Fe^{2+}, Co^{2+}, Zn^{2+}, Ni^{2+}, etc). The general chemical formula of inverse spinels family can be written in the form $\left(M_{1-x}^{2+}Fe_x^{3+}\right)_A\left[M_x^{2+}Fe_{2-x}^{3+}\right]_B O_4^{2-}$, where the parentheses represents the cations occupying tetrahedral A sites, whereas the brackets denote the cations occupying octahedral B sites in the spinel structure. The parameter x is the degree of inversion defined as the fraction of tetrahedral sites occupied by Fe^{3+} cations. Ideal bulk MFe_2O_4 is a fully inverse spinel ferrite ($x = 1$). The experimental determination of x is of vital importance because the physicochemical properties exhibited by the ferrites critically depend on this parameter.[1] Besides technological applications in spin-filtering[2] and multiferroic devices,[3,4] several biomedical applications on targeting, diagnosis, and disease treatment have also been reported. In addition, the cations M and Fe in the lattice respectively occupy the tetrahedral (1/8, 1/8, 1/8) sites, Wyckoff position 8a, and octahedral (1/2, 1/2, 1/2) sites, Wyckoff position 16d. Therefore, the single positional parameter u plus the unit-cell parameter a are sufficient to determine the spinel structure. It is known that altering the occupancies of the M and Fe sites can give rise to slight variations of the spinel structure, which can affect the corresponding nature and magnitude of superexchange interactions,[5] namely, A–A, B–B, and A–B, of which the A–B interactions tend to be highly significant.

Different types of ferrite-based composites have been studied, including magnetic ferrites composed of nonmagnetic oxides and polymers.[6–8] For practical applications, however, Fe_3O_4 is the most promising candidate due to its high Curie temperature, $T_C = 858$ K, as compared to other half metals. These characteristics of Fe_3O_4 can be utilized in the development of tunneling magnetoresistance based devices that would operate at room temperature with high efficiency.[9,10] Experimentally, the properties of ferrites are dependent on the synthesis technique and synthesis conditions.[11] $NiFe_2O_4$ has the inverse spinel structure in bulk form where divalent metal ions (Ni^{2+}) occupy octahedral sites and mixed spinel structure in case of nanoparticles where Ni^{2+} ions can occupy both tetrahedral and octahedral sites.[12] $CuFe_2O_4$ is ferromagnetically ordered for a weak magnetic field and it has wide applications due to its high thermal stability.[13] Nickel ferrite $NiFe_2O_4$ is a good example of inverse spinel ferrite and exhibits ferromagnetic nature with a Curie temperature of 858 K where half of the Fe^{3+} ions occupy the tetrahedral sites and the remaining ions occupy the octahedral sites, it is used in repulsive suspension for levitated railway systems, microwave absorber, magnetic liquids, magnetic refrigeration, and high density magnetic recording media.[14,15] In previous work,[16] the $CoFe_2O_4$ nanowire arrays become superparamagnetic at 600 K. High magnetostriction and strain-field derivative with low saturation field make (0 0 1) fiber textured $CoFe_2O_4$ attractive for sonar detector and force sensor applications.[17] Theoretically, the formation condition and energy of possible intrinsic point defects have been investigated by the first-principles calculations, and the effects of the intrinsic point defects on the electronic and magnetic properties of $CoFe_2O_4$ have been analyzed.[18] The experimental and numerical results using Monte Carlo simulation of the reduced magneti-

†Corresponding author. E-mail: rachidmasrour@hotmail.com

© 2019 Chinese Physical Society and IOP Publishing Ltd

zation and coercivity cobalt ferrite/polyvinylpyrrolidone are in relatively good agreement with each other.[19] The first-principles, mean-field, and series expansions calculations have been used to study the electronic and magnetic structures of Fe_3O_4.[20] Green's function theory has been used to study the magnetic properties of $Cu_xNi_{1-x}Fe_2O_4$ spinels.[21] The effect of Zn doping on magnetic properties of $MnFe_2O_4$ ferrite spinel has been studied by using high temperature series expansion combined with the Padé approximant and mean field theory.[22] In the previous work,[23] silicene is an intriguing two-dimensional (2D) topological material which is closely analogous to graphene but with stronger spin–orbit coupling effect and natural compatibility with current silicon-based electronic industry. It could realize a ferromagnetic phase, super-counter-fluidity phase, and antiferromagnetic phase of polarized light that are of interest for studying spin-dependent photon-photon interactions.[24] The effect of spin transport on nonlinear excitations was investigated in a ferromagnetic nanowire with nonuniform magnetizations.[25]

In the present work, we have used the Monte Carlo simulation to study the magnetic properties of inverse ferrite $\left(Fe^{3+}\right)\left[Fe^{3+}Co^{2+}\right]O_4^{2-}$, $\left(Fe^{3+}\right)\left[Fe^{3+}Cu^{2+}\right]O_4^{2-}$, $\left(Fe^{3+}\right)\left[Fe^{3+}Fe^{2+}\right]O_4^{2-}$, and $\left(Fe^{3+}\right)\left[Fe^{3+}Ni^{2+}\right]O_4^{2-}$ spinels. The critical and Curie Weiss temperatures are obtained for each system. The magnetic hysteresis cycles have been found for the four systems. The critical exponents associated with magnetization, magnetic susceptibility, and external magnetic field have been found.

2. Ising model

In inverse spinel ferrites $\left(Fe^{3+}\right)_A\left[Fe^{3+}Mn^{2+}\right]_B O_4^{2-}$, the B site is occupied by two types of ions, Mn^{2+} and Fe^{3+}, while the A site is occupied by Fe^{3+} ions. The Hamiltonian of the Ising system of inverse spinel ferrites with formula $Fe^{3+}(Fe^{3+}M^{2+})O_4$ (with M = Co, Cu, Fe, and Ni) in an external field $H_{\rm ext}$ may be put in the form

$$\begin{aligned} H = & -J'_{AA}\sum_{\langle i,j\rangle} \boldsymbol{S}_{Ai}\boldsymbol{S}_{Aj} - J'_{AB1}\sum_{\langle i,j\rangle} S_{Ai}\boldsymbol{\sigma}_{Bj} - J'_{AB2}\sum_{\langle i,k\rangle} S_{Ai}\boldsymbol{\sigma}_{Bk} \\ & - J'_{B1B1}\sum_{\langle j,l\rangle} \boldsymbol{\sigma}_{Bj}\boldsymbol{\sigma}_{Bl} - J'_{B1B2}\sum_{\langle j,m\rangle} \boldsymbol{\sigma}_{Bj}\boldsymbol{\sigma}_{Bm} \\ & - J'_{B2B2}\sum_{\langle m,n\rangle} \boldsymbol{\sigma}_{Bm}\boldsymbol{\sigma}_{Bn} - H_{\rm ext}\left(\sum_i S^z_{Ai} - \sum_j \sigma^z_{Bj}\right), \end{aligned} \tag{1}$$

with

$$\begin{aligned} J'_{AA} &= S_A \times S_A \times J_{AA}, \\ J'_{AB1} &= S_A \times \sigma_{B1} \times J_{AB1}, \\ J'_{AB2} &= S_A \times \sigma_{B2} \times J_{AB2}, \\ J'_{B1B1} &= \sigma_{B1} \times \sigma_{B1} \times J_{B1B1}, \\ J'_{B1B2} &= \sigma_{B1} \times \sigma_{B2} \times J_{B1B2}, \\ J'_{B2B2} &= \sigma_{B2} \times \sigma_{B2} \times J_{B2B2}, \end{aligned}$$

$S_A = Co^{2+} = 3/2$ or $S_A = Cu^{2+} = 1/2$ or $S_A = Fe^{2+} = 2$ or $S_A = Ni^{2+} = 1$, $S_{B2} = S_{B1} = Fe^{3+} = 5/2$.

The values of exchange interactions J_{AA}, J_{AB1}, J_{AB2}, J_{B1B1}, J_{B1B2}, and J_{B2B2} used in this work for four inverse ferrite $\left(Fe^{3+}\right)\left[Fe^{3+}Co^{2+}\right]O_4^{2-}$, $\left(Fe^{3+}\right)\left[Fe^{3+}Cu^{2+}\right]O_4^{2-}$, $\left(Fe^{3+}\right)\left[Fe^{3+}Fe^{2+}\right]O_4^{2-}$, and $\left(Fe^{3+}\right)\left[Fe^{3+}Ni^{2+}\right]O_4^{2-}$ spinels systems are given in Ref. [26] as listed in Table 1.

Table 1. The values of exchange interactions used in this work for the spinels.

Inverse spinels	J_{AA}/K[26]	J_{AB1}/K[26]	J_{AB2}/K[26]	J_{B1B1}/K[26]	J_{B1B2}/K[26]	J_{B2B2}/K[26]
$\left(Fe^{3+}\right)\left[Fe^{3+}Co^{2+}\right]O_4^{2-}$	–14	–28	–22.7	–9	–10.0	+46.0
$\left(Fe^{3+}\right)\left[Fe^{3+}Cu^{2+}\right]O_4^{2-}$	–14	–28	–27.0	–9	–10.0	+29.0
$\left(Fe^{3+}\right)\left[Fe^{3+}Fe^{2+}\right]O_4^{2-}$	–14	–28	–20.2	–9	–11.0	+44.0
$\left(Fe^{3+}\right)\left[Fe^{3+}Ni^{2+}\right]O_4^{2-}$	–14	–28	–27.4	–9	–10.0	+44.0

3. Monte Carlo simulations

The $Fe^{3+}(M^{2+}Fe^{3+})O_4$ is assumed to reside in the unit cells, and the system consists of total number of sites $N = N_A + N_B = 4096$, where N_A and N_B are the numbers of ions in site A and site B, respectively. We have used the Monte Carlo simulation to simulate the Hamiltonian given by Eq. (1). Periodic boundary conditions on the inverse ferrite spinels have been applied. Configurations have been generated by sequentially traversing the lattice and making single-spin flip attempts. Meanwhile, Monte Carlo update was performed by choosing random spins and then flipped with Boltzmann based probability. This can be done using the conventional Metropolis algorithm $P_{\rm Metro} = \exp(-\beta\Delta E)$ (where ΔE is the energy difference between the before and the after flip, $\beta = 1/k_{\rm B}T$ and $k_{\rm B}$ is the Bolzmann's constant, and T is the absolute temperature).[27] To obtain the numerical results, the data were generated with 5×10^5 Monte Carlo steps per spin where the first 5×10^4 Monte Carlo simulations are discarded and each Monte Carlo simulation started from a different initial condition.

The total internal energy is given by

$$E = \left\langle \frac{1}{N^3} H \right\rangle. \tag{2}$$

The magnetizations of spinels $Fe^{3+}(M^{2+}Fe^{3+})O_4$ (with M = Co, Cu, Fe, and Ni) are

$$M_A = \frac{1}{N_A} \sum_i \langle S_{Ai} \rangle, \tag{3}$$

$$M_B = \frac{1}{N_B} \sum_i \langle \sigma_{Bi} \rangle, \tag{4}$$

where S_i and σ_i are the magnetic spins of the i^{th} magnetic ions. The total magnetization is given by

$$M = \frac{N_A \times M_A + N_B \times M_B}{N_A + N_B}. \tag{5}$$

The corresponding magnetic susceptibilities χ are given by

$$\chi_A = \frac{\beta}{N_A} \left(\left\langle \sum_i S_{Ai}^2 \right\rangle - \left\langle \sum_i S_{Ai} \right\rangle^2 \right), \tag{6}$$

$$\chi_B = \frac{\beta}{N_B} \left(\left\langle \sum_i \sigma_{Bi}^2 \right\rangle - \left\langle \sum_i \sigma_{Bi} \right\rangle^2 \right), \tag{7}$$

$$\chi = \frac{N_A \times \chi_A + N_B \times \chi_B}{N_A + N_B}. \tag{8}$$

The critical exponents α, β, and γ associated with magnetization, magnetic susceptibility, and external magnetic field are given by

$$\begin{aligned} M &\approx (T_{\text{C}} - T)^{\beta}, \\ \chi &\approx (T - T_{\text{C}})^{-\gamma}, \\ M &\approx H_{\text{ext}}^{1/\delta}. \end{aligned} \tag{9}$$

4. Results and discussion

In the present work, we have used the Monte Carlo simulation to study the magnetic properties of inverse ferrite $\left(Fe^{3+}\right)\left[Fe^{3+}Co^{2+}\right]O_4^{2-}$, $\left(Fe^{3+}\right)\left[Fe^{3+}Cu^{2+}\right]O_4^{2-}$, $\left(Fe^{3+}\right)\left[Fe^{3+}Fe^{2+}\right]O_4^{2-}$, and $\left(Fe^{3+}\right)\left[Fe^{3+}Ni^{2+}\right]O_4^{2-}$ spinels. The critical temperatures T_{C} of $\left(Fe^{3+}\right)\left[Fe^{3+}Co^{2+}\right]O_4^{2-}$, $\left(Fe^{3+}\right)\left[Fe^{3+}Cu^{2+}\right]O_4^{2-}$, $\left(Fe^{3+}\right)\left[Fe^{3+}Fe^{2+}\right]O_4^{2-}$, and $\left(Fe^{3+}\right)\left[Fe^{3+}Ni^{2+}\right]O_4^{2-}$ are deduced from Figs. 1(a), 2(a), 3(a), and 4(a), respectively. The obtained values are given in Table 2. The Curie Weiss temperatures θ_{CW} are deduced from the inverse of magnetic susceptibilities for the four inverse ferrite spinels from Figs. 1(a), 2(a), 3(a), and 4(a), respectively (see Table 1). The obtained values of T_{C} and θ_{CW} are near to those obtained by experiment results[28,29] and the molecular-field approximation.[30]

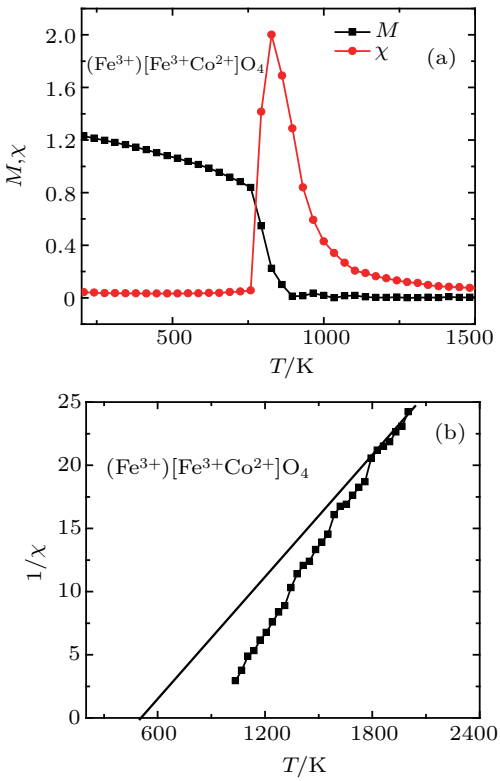


Fig. 1. (a) The thermal magnetization and magnetic susceptibility and (b) inverse magnetic susceptibility of $\left(Fe^{3+}\right)\left[Fe^{3+}Co^{2+}\right]O_4^{2-}$ spinels. The straight line in panel (b) is used to deduce the Curie Weiss temperature.

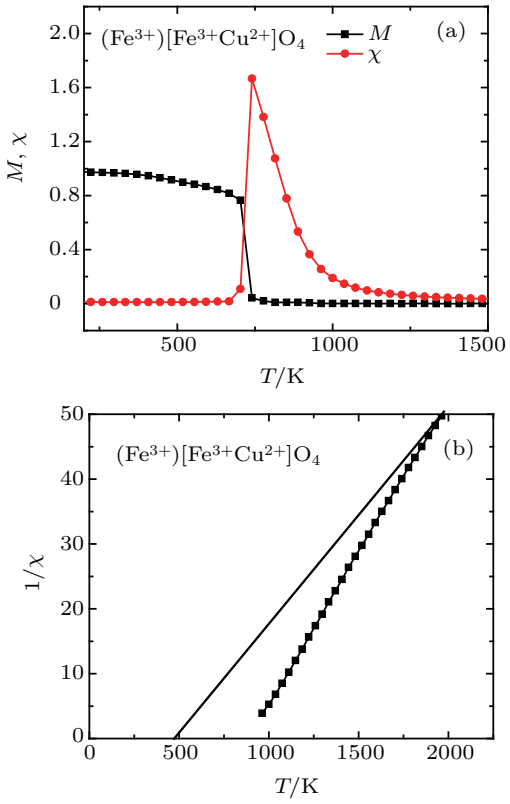


Fig. 2. (a) The thermal magnetization and magnetic susceptibility and (b) inverse magnetic susceptibility of $\left(Fe^{3+}\right)\left[Fe^{3+}Cu^{2+}\right]O_4^{2-}$ spinels. The straight line in panel (b) is used to deduce the Curie Weiss temperature.

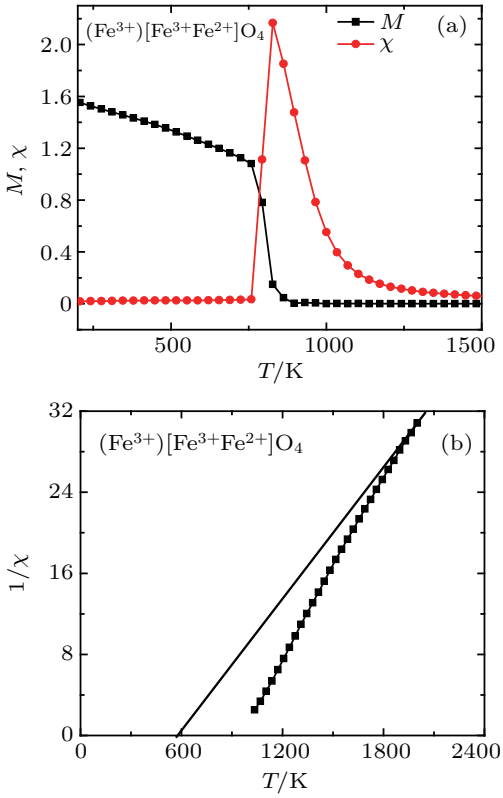


Fig. 3. (a) The thermal magnetization and magnetic susceptibility and (b) inverse magnetic susceptibility of $\left(Fe^{3+}\right)\left[Fe^{3+}Fe^{2+}\right]O_4^{2-}$ spinels. The straight line in panel (b) is used to deduce the Curie Weiss temperature.

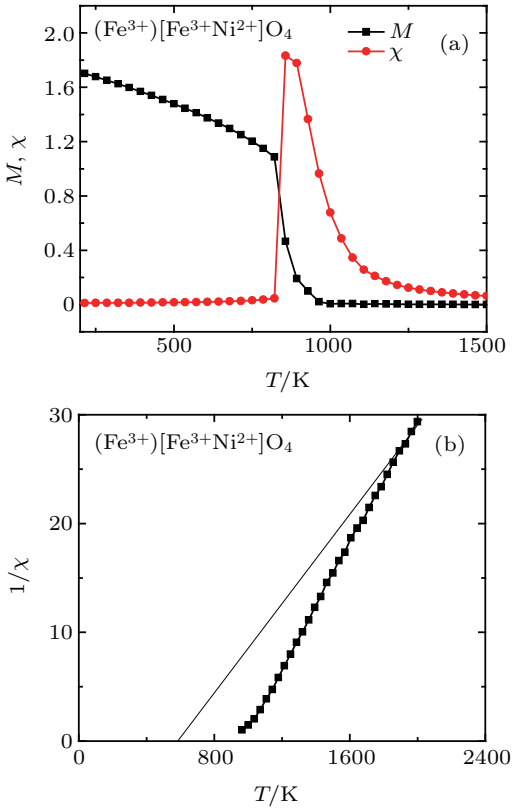


Fig. 4. (a) The thermal magnetization and magnetic susceptibility and (b) inverse magnetic susceptibility of $\left(Fe^{3+}\right)\left[Fe^{3+}Ni^{2+}\right]O_4^{2-}$ spinels. The straight line in panel (b) is used to deduce the Curie Weiss temperature.

Table 2. The critical and Curie Weiss temperatures obtained by Monte Carlo simulations, experiments (Ref. [25] for T_C and Ref. [29] for θ_{CW}), and molecular-field approximation[30] for the spinels.

Inverse spinels	T_C/K (Monte Carlo)	T_C/K (experiment[28])	T_C/K (molecular-field approximation[30])	θ_{CW}/K (Monte Carlo)	θ_{CW}/K (experiment[29])
$\left(Fe^{3+}\right)\left[Fe^{3+}Co^{2+}\right]O_4^{2-}$	830	793	826	888	520
$\left(Fe^{3+}\right)\left[Fe^{3+}Cu^{2+}\right]O_4^{2-}$	743	728	739	883	455
$\left(Fe^{3+}\right)\left[Fe^{3+}Fe^{2+}\right]O_4^{2-}$	834	858	858	784	585
$\left(Fe^{3+}\right)\left[Fe^{3+}Ni^{2+}\right]O_4^{2-}$	834	858	857	960	585

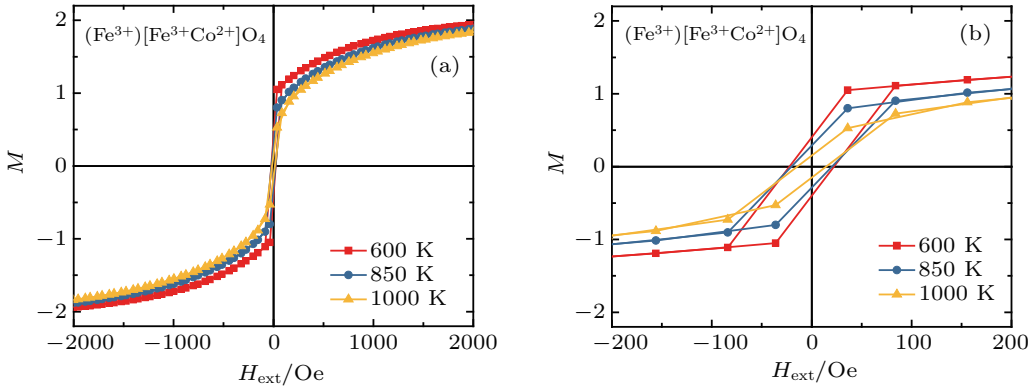


Fig. 5. (a) Magnetic $M(H_{ext})$ loop of $\left(Fe^{3+}\right)\left[Fe^{3+}Co^{2+}\right]O_4^{2-}$ for different temperatures $T = 600$ K, 850 K, and 1000 K, and (b) the enlarged low field region.

The magnetic $M(H_{ext})$ loops of $\left(Fe^{3+}\right)\left[Fe^{3+}Co^{2+}\right]O_4^{2-}$, $\left(Fe^{3+}\right)\left[Fe^{3+}Cu^{2+}\right]O_4^{2-}$, $\left(Fe^{3+}\right)\left[Fe^{3+}Fe^{2+}\right]O_4^{2-}$, and $\left(Fe^{3+}\right)\left[Fe^{3+}Ni^{2+}\right]O_4^{2-}$ spinels are shown in Figs. 7–10, respectively, for several values of temperatures $T = 600$ K, 850 K, and 1000 K. From these curves, we deduce that the magnetic coercive field, remanent magnetization, and satura-

tion magnetization decrease with increasing temperature (see Figs. 5(b), 6(b), 7(b), and 8(b)). This behavior is similar in magnetic properties of multilayer $BaTiO_3/NiFe_2O_4$ thin films prepared by solution deposition technique in Ref. [31]. The well saturated hysteresis loops are recorded in the range from 0.2 T to −0.2 T (Figs. 5–8) and their shapes resemble the ferrimagnetic behavior typical for cobalt (or nickel, copper-iron) ferrite based materials.

Figures 9–11 present the magnetic $M(H_{\text{ext}})$ loop of $\left(Fe^{3+}\right)\left[Fe^{3+}Co^{2+}\right]O_4^{2-}$, $\left(Fe^{3+}\right)\left[Fe^{3+}Cu^{2+}\right]O_4^{2-}$, $\left(Fe^{3+}\right)\left[Fe^{3+}Fe^{2+}\right]O_4^{2-}$, and $\left(Fe^{3+}\right)\left[Fe^{3+}Ni^{2+}\right]O_4^{2-}$ for temperatures $T = 600$ K, 850 K, and 1000 K, respectively. The saturation magnetization and the magnetic coercive field decrease as the number of electrons in the valence shell of the magnetic atom (3d) increase, such as given in the periodic table. For a weak external magnetic field, the four systems present the ferromagnetical order and the superparamagnetic order for a higher external magnetic field such as given in Ref. [13].

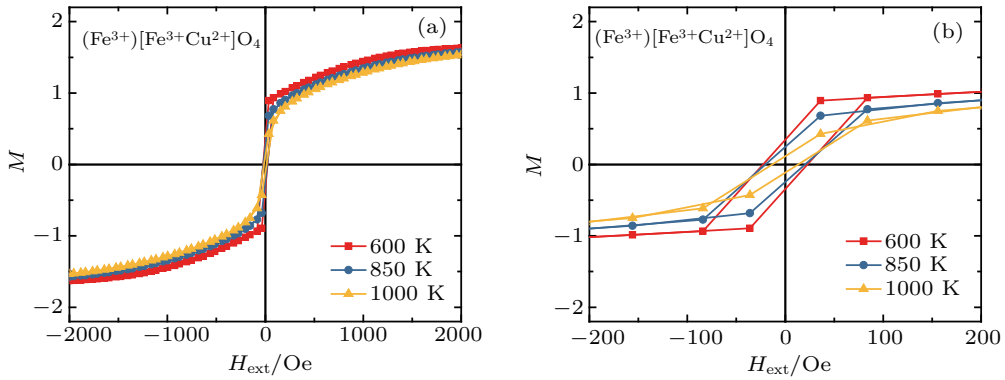


Fig. 6. (a) Magnetic $M(H_{\text{ext}})$ loop of $\left(Fe^{3+}\right)\left[Fe^{3+}Cu^{2+}\right]O_4^{2-}$ for different temperatures $T = 600$ K, 850 K, and 1000 K, and (b) the enlarged low field region.

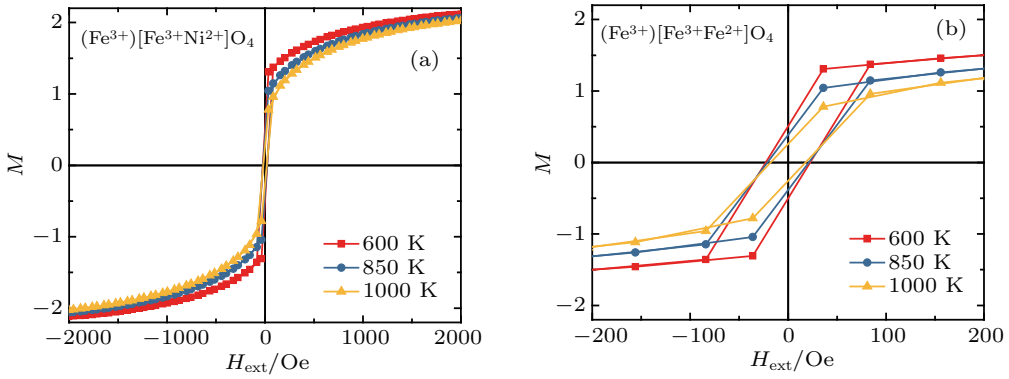


Fig. 7. (a) Magnetic $M(H_{\text{ext}})$ loop of $\left(Fe^{3+}\right)\left[Fe^{3+}Fe^{2+}\right]O_4^{2-}$ for temperatures $T = 600$ K, 850 K, and 1000 K, and (b) the enlarged low field region.

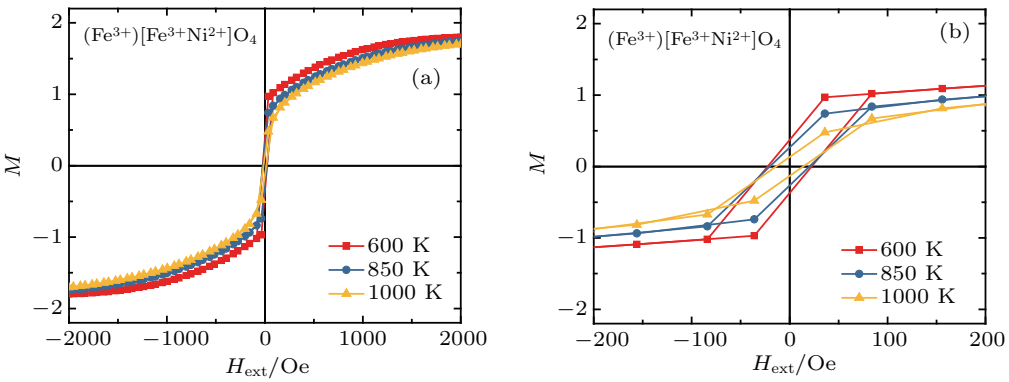


Fig. 8. (a) Magnetic $M(H_{\text{ext}})$ loop of $\left(Fe^{3+}\right)\left[Fe^{3+}Ni^{2+}\right]O_4^{2-}$ for different temperatures $T = 600$ K, 850 K, and 1000 K, and (b) the enlarged low field region.

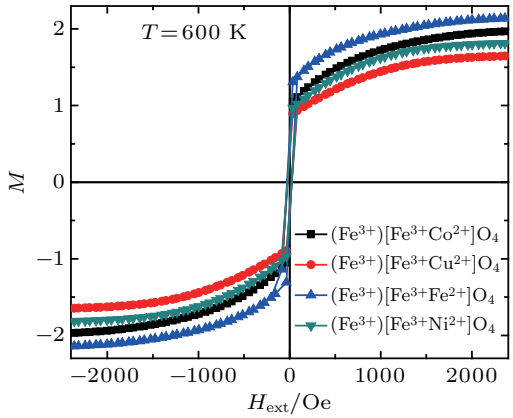


Fig. 9. Magnetic $M(H_{\rm ext})$ loops of $\left(Fe^{3+}\right)\left[Fe^{3+}Co^{2+}\right]O_4^{2-}$, $\left(Fe^{3+}\right)\left[Fe^{3+}Cu^{2+}\right]O_4^{2-}$, $\left(Fe^{3+}\right)\left[Fe^{3+}Fe^{2+}\right]O_4^{2-}$, and $\left(Fe^{3+}\right)\left[Fe^{3+}Ni^{2+}\right]O_4^{2-}$ at temperature $T = 600$ K.

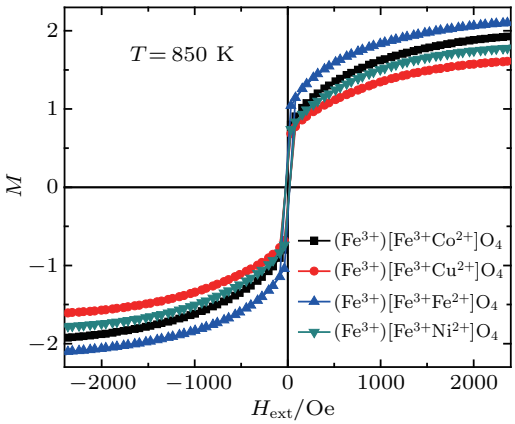


Fig. 10. Magnetic $M(H_{\rm ext})$ loops of $\left(Fe^{3+}\right)\left[Fe^{3+}Co^{2+}\right]O_4^{2-}$, $\left(Fe^{3+}\right)\left[Fe^{3+}Cu^{2+}\right]O_4^{2-}$, $\left(Fe^{3+}\right)\left[Fe^{3+}Fe^{2+}\right]O_4^{2-}$, and $\left(Fe^{3+}\right)\left[Fe^{3+}Ni^{2+}\right]O_4^{2-}$ at temperature $T = 850$ K.

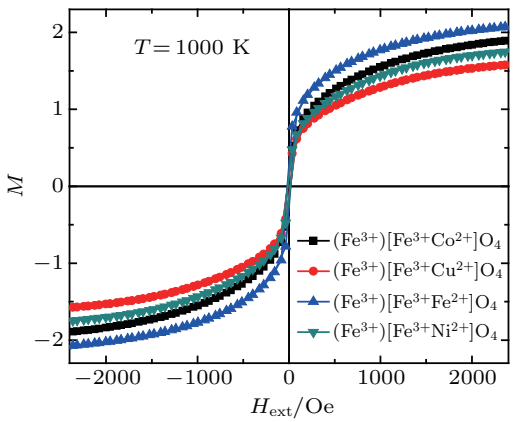


Fig. 11. Magnetic $M(H_{\rm ext})$ loops of $\left(Fe^{3+}\right)\left[Fe^{3+}Co^{2+}\right]O_4^{2-}$, $\left(Fe^{3+}\right)\left[Fe^{3+}Cu^{2+}\right]O_4^{2-}$, $\left(Fe^{3+}\right)\left[Fe^{3+}Fe^{2+}\right]O_4^{2-}$, and $\left(Fe^{3+}\right)\left[Fe^{3+}Ni^{2+}\right]O_4^{2-}$ at temperature $T = 1000$ K.

We have calculated the critical exponents β, γ, and δ associated with the magnetization, magnetic susceptibility, and external magnetic field using Eq. (7). The obtained values of β, γ, and δ are given in Table 3. The obtained values are comparable with those given by 3D Ising model ($\beta = 0.22$, $\gamma = 1.24$, and $\delta = 4.78$).[31–37]

Table 3. The critical exponents β, γ, and δ associated with the magnetization, magnetic susceptibility, and external magnetic field of the spinels.

Inverse spinels	β	γ	δ
$\left(Fe^{3+}\right)\left[Fe^{3+}Co^{2+}\right]O_4^{2-}$	0.202	1.234	4.765
$\left(Fe^{3+}\right)\left[Fe^{3+}Cu^{2+}\right]O_4^{2-}$	0.257	1.267	4.782
$\left(Fe^{3+}\right)\left[Fe^{3+}Fe^{2+}\right]O_4^{2-}$	0.212	1.233	4.764
$\left(Fe^{3+}\right)\left[Fe^{3+}Ni^{2+}\right]O_4^{2-}$	0.222	1.243	4.773

5. Conclusion

The magnetic properties of inverse ferrite $\left(Fe^{3+}\right)\left[Fe^{3+}Co^{2+}\right]O_4^{2-}$, $\left(Fe^{3+}\right)\left[Fe^{3+}Cu^{2+}\right]O_4^{2-}$, $\left(Fe^{3+}\right)\left[Fe^{3+}Fe^{2+}\right]O_4^{2-}$, and $\left(Fe^{3+}\right)\left[Fe^{3+}Ni^{2+}\right]O_4^{2-}$ spinels are investigated. The critical temperatures and the Curie Weiss temperatures are found using Monte Carlo simulation. The obtained values of $T_{\rm C}$ and $\theta_{\rm CW}$ are near to those obtained by experiments. The magnetic coercive filed, remanent magnetization, and saturation magnetization decrease with increasing temperature. The critical exponents β, γ, and δ are deduced. The obtained values are comparable with those given by 3D Ising model.[31–37]

References

[1] Tamayo H S, García K E and Barrero C A 2019 *J. Magn. Magn. Mater.* **471** 242

[2] Ramos A V, Guittet M J, Moussy J B, Mattana R, Deranlot C, Petroff F and Gatel C 2007 *Appl. Phys. Lett.* **91** 122107

[3] Zheng H, Wang J, Lofl, S E, Ma Z, Ardabili L M, Zhao T, Riba L S, Shinde S R, Ogale S B, Bai F, Viehl, D, Jia Y, Schlom D G, Wuttig M, Roytburd A and Ramesh R 2004 *Science* **303** 661

[4] Wu Y, Wan J G, Liu J M and Wang G 2010 *Appl. Phys. Lett.* **96** 152902

[5] Kodama R H, Berkowitz A E, McNiff Jr E J and Foner S 1997 *J. Appl. Phys.* **81** 5552

[6] Wang J, Luo J, Fan Q, Suzuki M, Suzuki I S, Engelhard M H, Lin Y, Kim N, Wang J Q and Zhong C J 2005 *J. Phys. Chem. B* **109** 21593

[7] Casu A, Casula M F, Corrias A, Falqui A, Loche D and Marras S 2007 *J. Phys. Chem. C* **111** 916

[8] Murillo N, Ochoteco E, Alesanco Y, Pomposo J A, Rodriguez J, Gonzalez J, Val J J D, Gonzalez J M, Brtel M R and Lopez A R A 2004 *Nanotechnology* **15** S322

[9] Zhang Z and Satpathy S 1991 *Phys. Rev. B* **44** 13319

[10] Yanase A and Siratori K 1984 *J. Phys. Soc. Jpn.* **53** 312

[11] Joshi S, Kumar M, Pandey H, Singh M and Pal P 2018 *J. Alloys Compnds.* **768** 287

[12] Joshi S, Kumar M, Chhoker S, Srivastava G, Jewariya M and Singh V N 2014 *J. Mol. Struct* **1076** 55

[13] Ahmed Y M Z, Hessien M M, Rashad M M and Ibrahim I A 2009 *J. Magn. Magn. Mater.* **321** 181

[14] Ramankutty C G and Sugunan S 2001 *Appl. Catal. A* **218** 39

[15] Reddy C V G, Manorama S V and Rao V 1999 *J. Sens. Actuators B: Chemical.* **55** 90

[16] Yuan J J, Zhao Q, Xu Y S, Liu Z G, Du X B and Wen G H 2009 *J. Magn. Magn. Mater.* **321** 2795

[17] Wang J, Li J, Li X, Bao X and Gao X 2018 *J. Magn. Magn. Mater.* **462** 53

[18] Huang Y L, Fan W B, Hou Y H, Guo K X, Ouyang Y F and Liu Z W 2017 *J. Magn. Magn. Mater.* **429** 263

[19] Mirzaee Sh, shayesteh S F, Mahdavifar S and Hekmatara S H 2015 *J. Magn. Magn. Mater.* **393** 1

[20] Masrour R, Hlil E K, Hamedoun M, Benyoussef A, Mounkachi O and El Moussaoui H 2015 *J. Magn. Magn. Mater.* **378** 37

[21] Salmi S, Masrour R, El Grini A, Bouslykhane K, Hourmatallah A, Benzakour N and Hamedoun M 2018 *J. Cluster Sci.* **29** 493
[22] Masrour R, Hamedoun M and Benyoussef A 2011 *Chem. Phys. Lett.* **513** 280
[23] Zhang X L, Liu Z F and Liu W M 2013 *Sci. Rep.* **3** 2908
[24] Ji A C, Xie X C and Liu W M 2007 *Phys. Rev. Lett.* **99** 183602
[25] He P B and Liu W M 2005 *Phys. Rev. B* **72** 064410
[26] Srivastava C M, Srinivasan G and Nanadikar N G 1979 *Phys. Rev. B* **19** 499
[27] Metropolis N, Rosenbluth A W, Rosenbluth M N, Teller A H and Teller E 1953 *J. Chem. Phys.* **21** 1087
[28] Smit J and Wijn H P J 1959 *Ferrites* p. 143 (New York: Wiley)
[29] Benenson W, Harris J W, Stöcker H and Lutz H 2002 *Handbook of Physics* (Berlin: Springer-Verlag)
[30] Bercoff P G and Bertorello H R 1997 *J. Magn. Magn. Mater.* **169** 314
[31] Goldner L S and Ahlers G 1992 *Phys. Rev. B* **45** 13129
[32] Le Guillou J C and Zinn-Justin J 1985 *J. Phys. Lett.* **46** 137
[33] Baillie C F, Gupta R, Hawick K A and Pawley G S 1992 *Phys. Rev. B* **45** 10438
[34] Ferrenberg, A M and Landau D P 1991 *Phys. Rev. B* **44** 5081
[35] Adler J 1983 *J. Phys. A* **16** 3585
[36] Baker G A J, Nickel B G and Meiron D I 1978 *Phys. Rev. B* **17** 1365
[37] George M J and Rehr J 1984 *Phys. Rev. Lett.* **53** 2063